Electron-spin-resonance investigation of the heavy-fermion compound $Ce(Cu_{1-x}Ni_x)_2Ge_2$

H.-A. Krug von Nidda, A. Schütz, M. Heil, and B. Elschner

Institut für Festkörperphysik, TU Darmstadt, Hochschulstrasse 6, D-64289 Darmstadt, Germany

A. Loidl

Experimentalphysik V, Universität Augsburg, D-86135 Augsburg, Germany
(Received 20 August 1997)

The heavy-fermion compound $Ce(Cu_{1-x}Ni_x)_2Ge_2$ is investigated by Gd^{3+} electron spin resonance (ESR) within the whole concentration range ($0 \leq x \leq 1$). The Kondo-lattice system exhibits an alloying-induced transition from an antiferromagnetically ordered heavy-fermion ground state ($x=0$) to pure Kondo-like behavior with strongly enhanced effective masses ($x=1$). The temperature dependence of the ESR linewidth ΔH allows one to distinguish between the different ground states. The nature of the magnetic order changes significantly from concentrations $x \lesssim 0.5$ to $x > 0.5$. The ESR data provide some further experimental evidence for a transition from a local-moment type ($x < 0.5$) to some kind of itinerant heavy-fermion band magnetism ($0.5 < x < 0.8$). Non-Fermi-liquid behavior is discussed for $x=0.8$ where the magnetism is suppressed. Our results agree very well with the ^{63}Cu NMR spin-lattice relaxation rate $1/T_1$ and the dynamic structure factor $S(\mathbf{Q}, \omega)$ obtained from inelastic neutron-scattering experiments. [S0163-1829(98)04918-2]

I. INTRODUCTION

The pseudoternary heavy-fermion system $Ce(Cu_{1-x}Ni_x)_2Ge_2$ has been subject to intensive experimental and theoretical studies concerning the physics of highly correlated electrons during the last years.[1] Heavy fermions (or more generally Kondo lattices) are intermetallic compounds containing elements with partially filled $4f$ or $5f$ shells (e.g., Ce, Yb, U) on regular lattice sites.[2] The hybridization strength $JN(E_F)$ of the local f moments with the conduction electrons is responsible for the correlation effects observed at low temperatures. [Here J denotes the exchange coupling, and $N(E_F)$ is the electronic density of states at the Fermi energy.] This hybridization gives rise for two competing processes which determine the ground-state properties of Kondo lattices. For large J the dominant mechanism is the Kondo screening of the f moments by the band states with its characteristic Kondo-lattice temperature $T^* \propto \exp[-1/JN(E_F)]$. The Kondo effect increases the density of states near E_F and generates a coherent Fermi-liquid ground state of heavy quasiparticles for $T < T^*$. For small J the important process is the RKKY interaction between the f moments, which is transferred via the conduction electrons. Its typical energy scale is given by $T_{RKKY} \propto [JN(E_F)]^2$. This indirect exchange interaction leads to a magnetically ordered ground state at $T < T_{RKKY}$.[3]

For $Ce(Cu_{1-x}Ni_x)_2Ge_2$, which belongs to the tetragonal $ThCr_2Si_2$ homologues (like $CeCu_2Si_2$), the energy scales of Kondo screening and the RKKY interaction are of comparable magnitude, and therefore the ground state of the system is very sensitive to changes in the composition x. The schematic phase diagram shown in Fig. 1 was obtained from susceptibility, resistivity, specific-heat, thermal expansion, thermopower, and quasielastic neutron-scattering measurements:[1] $CeCu_2Ge_2$, with a unit-cell volume $V = 177$ Å³, is an antiferromagnetically ordered heavy-fermion sys-

tem with $T^* = 6$ K and a Néel temperature $T_{N1} = 4.1$ K. Here Kondo screening and the RKKY interaction are of nearly equal strength ($T^* \approx T_{RKKY}$). Replacing copper by nickel increases the hybridization by decreasing the volume of the unit cell linearly down to $V = 170$ Å³ for $CeNi_2Ge_2$, which exhibits a nonmagnetic heavy-fermion ground state with a characteristic temperature $T^* = 30$ K ($T^* \gg T_{RKKY}$). With increasing x the first antiferromagnetic phase (T_{N1}) which is of local moment type is suppressed and a second ordered phase
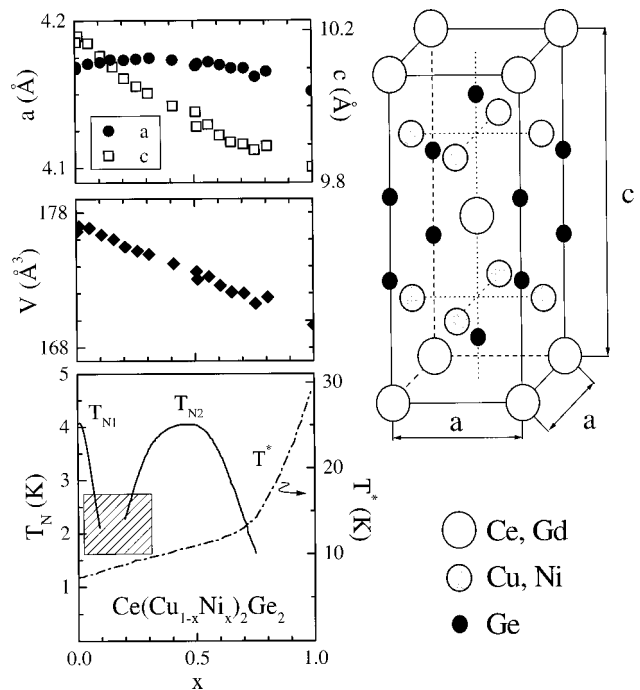

FIG. 1. Crystal structure, lattice parameters a and c, volume V of the unit cell, and phase diagram: T^* denotes the Kondo-lattice temperature; the two magnetic phase transitions T_{N1} and T_{N2} overlap within the dashed area.

(T_{N2}) develops within the dashed area in which an overlap of both phases is indicated by different experimental results.[1] T_{N2} passes a maximum value of 4.1 K at $x=0.5$. For $x > 0.5$ the ordered moment strongly decreases, and for $x = 0.65$ it cannot be detected by neutron diffraction anymore. The appearance of band magnetism of heavy quasiparticles for $x>0.5$ has been proposed.[1,4] At $x=0.8$ the magnetic order disappears ($T_N \rightarrow 0$), and the occurrence of non-Fermi-liquid behavior is discussed, as this compound is close to a magnetic instability.[5,6] The phase diagram of the compound $Ce(Cu_{1-x}Ni_x)_2Ge_2$ obviously cannot be explained by the volume effect alone, because the first depression of the ordering temperature within the dashed area is not observed, if one applies hydrostatic pressure to $CeCu_2Ge_2$. After continuous suppression of the magnetism, superconductivity is induced for pressures >70 kbar,[7] which is also observed at ambient pressure in $CeCu_2Si_2$ below $T_c=0.7$ K, but not in $CeNi_2Ge_2$. To understand the phase diagram in full detail, one has to take into account the different electronic configurations of nickel with respect to copper which modifies the band structure as well.

Electron-spin-resonance (ESR) experiments on single crystals of Gd-doped $CeCu_2Si_2$ were performed some years ago.[8] Gd substitution is necessary, as the $4f^1$ moment of the Ce ion relaxes much too fast to yield any measurable ESR signal. It has been shown that the Gd^{3+} probe (spin $S=7/2$, angular momentum $L=0$) which occupies the cerium site couples to the spin fluctuations of the Ce $4f$ moments via RKKY interactions, yielding a characteristic temperature dependence of the Gd^{3+} ESR linewidth. In this paper we present our recent Gd^{3+} ESR results in the whole concentration range $0 \leq x \leq 1$ using oriented powder samples, because Gd-doped single crystals are hard to grow and were not available. We document that Gd^{3+} ESR is sensitive to the different ground states and yields comparable results to ^{63}Cu NMR and quasielastic neutron scattering.

II. SAMPLE PREPARATION AND EXPERIMENTAL SETUP

Polycrystalline samples of $Ce_{1-y}Gd_y(Cu_{1-x}Ni_x)_2Ge_2$ ($y \leq 2\%$) were melted together stoichiometrically from the elements (purity better than 99.99%) in an argon-arc furnace and annealed for 2 days at 1223 K. X-ray-diffraction and microprobe analysis proved the proper $ThCr_2Si_2$ structure and did not reveal any parasitic phases. As the paramagnetic susceptibility of these compounds shows its maximum value in the direction of the crystallographic c axis, it was easy to prepare oriented powder samples: The polycrystals were powdered to nearly single-crystalline grains of a diameter smaller than 40 μm, immersed in liquified paraffin, and oriented along the crystallographic c axis within a static magnetic field of 20 kOe.

The ESR measurements were performed with a Varian E-101 spectrometer working at $\nu=9.2$ GHz in the temperature range 1.5 K $\leq T \leq 300$ K. For cooling a continuous-flow helium cryostat (Oxford Instruments) was used for $T > 4.2$ K and a cold-finger bath cryostat below liquid-helium temperatures. The magnetic field was controlled by a temperature stabilized Hall probe (Bruker).
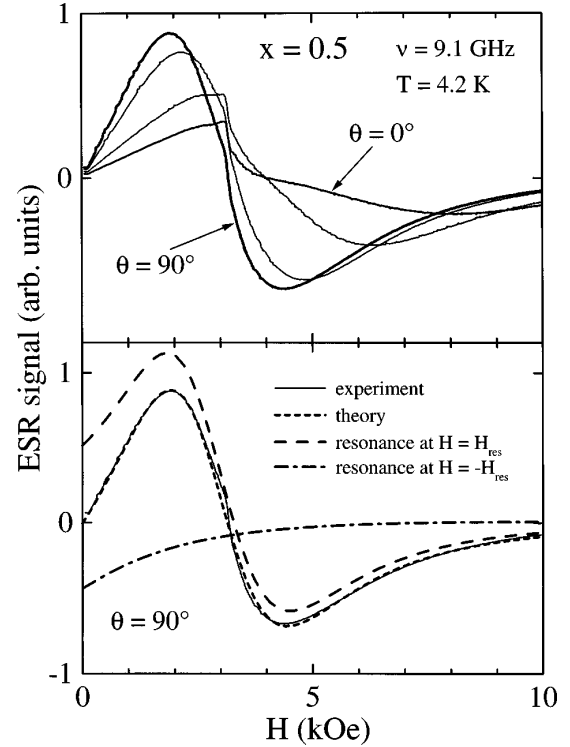

FIG. 2. Upper frame: ESR spectra from oriented powder samples of $Ce(Cu_{0.5}Ni_{0.5})_2Ge_2$ doped with 2% Gd for different orientations ($\vartheta=0°$, 30°, 60°, 90°) at 4.2 K. The distortions at 3.3 kOe originate from the background of the cavity. Lower frame: fit with a Dysonian line shape (short dashed) according to Eq. (1). The dashed and dash-dotted lines show the contributions of both circular polarization components as described in the text.

III. RESULTS

A. ESR spectra

Electron spin resonance measures the absorption P_{abs} of the transversal magnetic microwave field (frequency ν) as a function of the static magnetic field **H**. To improve the signal-to-noise ratio, one detects the derivation of the absorption dP_{abs}/dH with a lock-in technique. All compounds ($0 \leq x \leq 1$) show a broad resonance line which strongly depends on the polar angle ϑ between the crystallographic c axis and the static magnetic field **H**, as shown for $x=0.5$ in the upper frame of Fig. 2. The distortion of the spectra at 3.3 kOe originates from the background of the cavity. For angles $\vartheta > 30°$ the spectrum (lower frame of Fig. 2) is well fitted by a single resonance line of Dysonian shape.[9] As in the compounds under consideration the ESR linewidth is of the same order of magnitude as the resonance field, one has to take into account both circular polarization components of the linearly polarized exciting microwave field. This yields a contribution of the right circular resonance which is centered at the reversed magnetic field with respect to the left circular resonance. Therefore the complete fit formula of the ESR signal is given by

$$\frac{d}{dH}P_{abs} \propto \frac{d}{dH}\left\{\frac{\Delta H + \alpha(H - H_{res})}{(H - H_{res})^2 + \Delta H^2} + \frac{\Delta H + \alpha(H + H_{res})}{(H + H_{res})^2 + \Delta H^2}\right\},$$

(1)

where H_{res} denotes the resonance field and ΔH the half line-width at half of the maximum absorption. Equation (1) describes a Lorenzian line which includes both absorption χ''_{Gd} and dispersion χ'_{Gd} ($0 \leq \alpha \leq 1$), because the skin effect drives electric and magnetic microwave components out of phase in metals.[10] The dispersion-to-absorption ratio α was used as the fit parameter. For samples large compared to the skin depth of the microwave field, one finds an asymmetric line shape with $\alpha = 1$, whereas for very small samples α reaches zero, describing a symmetric resonance line as in dielectrics.

The linewidth ΔH reaches its minimum value for $\vartheta = 90°$. At small angles $\vartheta < 30°$, the spectrum becomes very broad and deviates from the Dysonian shape. To understand the observed ESR spectra (Fig. 2) and the angular dependence of resonance field and linewidth (Fig. 3), one has to consider the spin Hamiltonian for the Gd^{3+} probe in a metal with tetragonal crystal symmetry (dominant uniaxial term) given by[11]

$$\mathcal{H} = \mu_B \mathbf{H}g\mathbf{S} + \tfrac{1}{3}b_2^0[3S_z^2 - S(S+1)] + J_{\text{Gd}}\mathbf{S}\cdot\boldsymbol{\sigma}. \quad (2)$$

The first term describes the Zeeman interaction of the Gd spin $\mathbf{S}$ with the static magnetic field $\mathbf{H}$ (μ_B is the Bohr magneton and g the gyromagnetic tensor, which is assumed to be isotropic $g = 2$). The second term is caused by the axial crystal electric field (parameter b_2^0). The crystal-field contributions of higher order are neglected, because they are at least 10 times smaller than the uniaxial contribution.[8] The third part of the Hamiltonian is the exchange interaction between the Gd^{3+} ion and the conduction electrons with spin density $\boldsymbol{\sigma}$ where J_{Gd} denotes the exchange integral.

The Zeeman term alone splits the $^8S_{7/2}$ ground state of the Gd^{3+} ion into eight equidistant energy levels $E_m = g\mu_B Hm$ ($-7/2 \leq m \leq 7/2$). The microwave (frequency ν) induces magnetic dipole transitions $\Delta m = \pm 1$ between them, showing a single resonance absorption for $h\nu = g\mu_B H_{\text{res}}$ (h denotes the Planck constant) as the ESR spectrum.

The crystal electric field shifts the energy levels against each other. For $b_2^0 \ll h\nu$ the eigenvalues of the sum of Zeeman and crystal-field operator are approximated by $E_m = g\mu_B Hm + \tfrac{1}{3}b_2^0[3m^2 - S(S+1)]\tfrac{1}{2}(3\cos^2\vartheta - 1)$, yielding the resonance positions $g\mu_B H_{m \rightarrow m+1} = h\nu - \tfrac{1}{2}b_2^0(2m+1)(3\cos^2\vartheta - 1)$, which coincide at the magic angle $\vartheta = 54.7°$. At $\vartheta = 0°$, where these expressions hold exactly for all values of b_2^0, the largest crystal-field splitting of the spectrum occurs with a distance of $2b_2^0$ between neighboring resonances. For larger values of $b_2^0 \lesssim h\nu$, one has to diagonalize the sum of Zeeman and crystal-field terms and to determine the transitions numerically, whereby one has to take into account all possible 28 transitions. Simulations show that in this case the overall splitting does not vanish at any angle, but reaches its smallest values for $\vartheta > 50°$, where it changes only slightly up to $\vartheta = 90°$.

The scattering of the conduction electrons at the Gd spin (exchange interaction) couples all the transitions and narrows the ESR spectrum (comparable to the motional narrowing observed in NMR experiments).[12,13] In the case of a strong exchange narrowing the spectrum again consists of one single resonance line. But the crystal field remains visible in

the orientation dependence of resonance field H_{res} and linewidth ΔH: The resonance field is given by the first moment of all fine-structure transitions,[13]

$$H_{\text{res}} = \sum_m P_m H_{m \rightarrow m+1}, \quad (3)$$

where

$$P_m = \frac{c_m \exp(-E_m/k_B T)}{\sum_{m'} c_{m'} \exp(-E_{m'}/k_B T)}.$$

For $b_2^0 \ll h\nu$ the transition probability is approximated by $c_m = S(S+1) - m(m+1)$. For larger $b_2^0 \lesssim h\nu$ the coefficients c_m have to be computed numerically. The linewidth depends on the second moment of all transitions,[13]

$$\Delta H = \Delta H_0 + \Delta H_R + \frac{1}{\delta}\sum_m P_m(H_{m \rightarrow m+1} - H_{\text{res}})^2. \quad (4)$$

ΔH_R is the linewidth caused by relaxation processes, ΔH_0 is a constant residual linewidth originating from impurities and lattice defects, and the factor $1/\delta$ is a function of ΔH_R itself. For a small fine-structure splitting compared with the relaxation $\mu_B \Delta H_R \gg b_2^0$, one obtains $\delta \approx (2 + \Theta_{\text{Gd}}/T)\Delta H_R$.[12] The Curie temperature Θ_{Gd} of the Gd doping is assumed to be zero for small Gd concentrations.

For larger fine-structure splittings $b_2^0 \lesssim \mu_B \Delta H_R$, the spectrum is only partially exchange narrowed. Therefore especially those transitions which are far away from the first moment of all transitions do not take part in the narrowing process. This must be taken into account concerning the first and second moments of the exchange-narrowed spectrum in Eqs. (3) and (4). The distortion of the ESR signal at low angles ϑ, where the fine-structure splitting is maximal, shows that we deal with partially exchange-narrowed spectra in our experiments. Nevertheless, we tried to estimate the axial crystal-field parameter b_2^0 using formulas (3) and (4) as an approximation regarding especially the strong transitions.[14] For $x = 0.5$ the result is shown in Fig. 3: The orientation dependence of the resonance field H_{res} (upper frame) and linewidth ΔH (lower frame) is well described by $b_2^0/h = 1.6$ GHz with $g = 1.85$, $\Delta H_0 = 1.0$ kOe, and $\Delta H_R = 0.8$ kOe. The g value is obviously too small. This can be understood because of the deviations of the spectra at low angles from the Dysonian line shape, where the fits are not very reliable. Furthermore, ΔH_0 is probably overestimated compared to ΔH_R, because we used the approximation $\delta \approx 2\Delta H_R$ at all angles ϑ. But δ is expected to decrease at low angles, as it characterizes the strength of the narrowing process which weakens with increasing fine-structure splitting.

Similar estimations for the other compounds yield a monotonously increasing b_2^0 with increasing x. For $x < 0.7$ it changes only slightly, but for $x > 0.7$ it increases up to 2.8 GHz at $x = 1$.

B. Temperature dependence of the ESR linewidth

Because of the strong influence of the crystal field on the resonance field and the uncertainties concerning the determination of the crystal-field parameter b_2^0, it is very difficult to obtain reliable g values. Therefore we confine ourselves to a
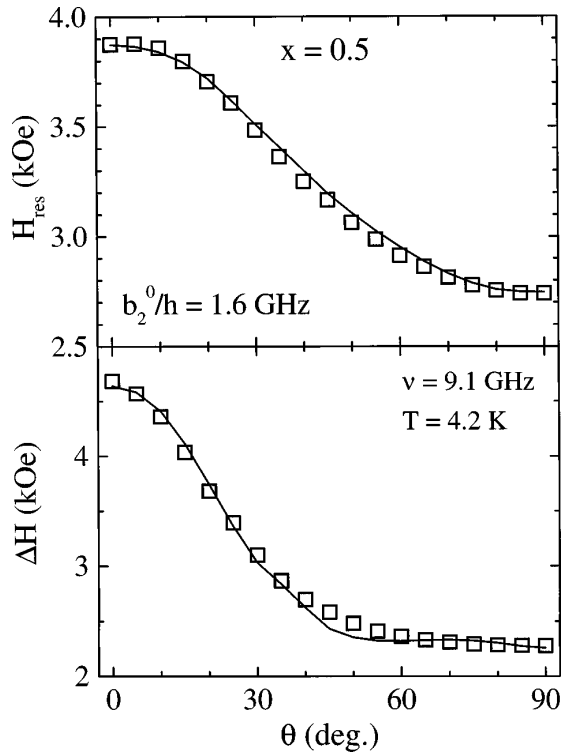
FIG. 3. Resonance field H_{res} (upper frame) and linewidth ΔH (lower frame) as a function of the polar angle ϑ for Ce(Cu$_{0.5}$Ni$_{0.5}$)$_2$Ge$_2$ doped with 2% Gd at 4.2 K: open squares, experimental values; lines, fits according to Eqs. (3) and (4) as described in the text.
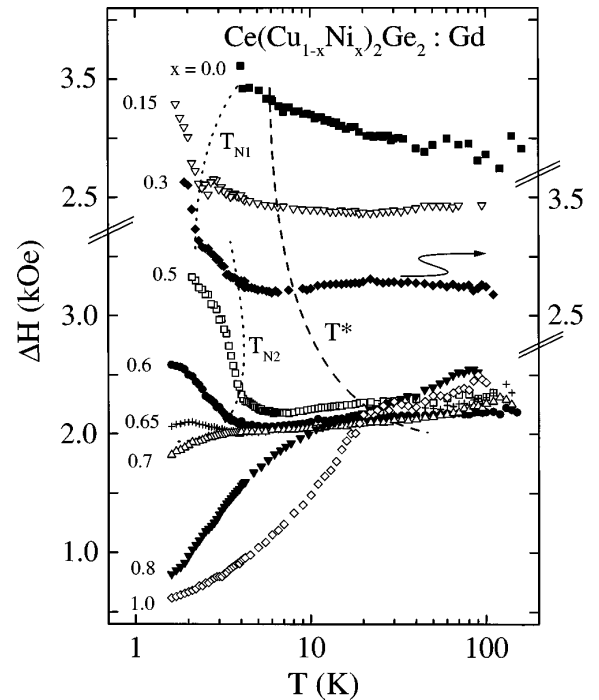

FIG. 4. Linewidth ΔH as a function of the temperature T for different concentrations x at the angle $\vartheta = 90°$. The dashed line marks T^*, and the dotted lines indicate T_{N1} and T_{N2}. The logarithmic temperature scale yields a better resolution of the behavior at low temperatures. Note that the experimental values have been shifted vertically.

discussion of the linewidth ΔH at the orientation $\vartheta = 90°$, where the spectrum reveals the largest exchange narrowing. Figure 4 shows the linewidth as a function of temperature for the whole concentration range $0 \leqslant x \leqslant 1$. We have chosen a logarithmic temperature scale, because this yields a better resolution at low temperatures. For $x=0$ the resonance line is very broad at all temperatures. The linewidth ΔH increases with decreasing temperature from 2.9 kOe at 100 K to 3.4 kOe just above $T_{N1} = 4.1$ K. Below the ordering temperature the line strongly broadens and vanishes so that a reasonable fit is no longer possible. For $x = 0.15$ the behavior is qualitatively similar with slightly smaller ΔH. Again, a strong line broadening is observed below $T_{N1} \approx 2.5$ K. The concentration $x = 0.3$ exhibits a slight minimum of the linewidth with decreasing temperature below T^*. The broadening at $T_{N2} \approx 3.5$ K is followed by a second transition at about 2.4 K, which perhaps can be labeled T_{N1}, as it shows a comparable broadening behavior as $x = 0.15$. The existence of two transitions is supported by magnetic susceptibility data reported for the compound $x = 0.25$,[1] where also two anomalies have been observed at comparable temperatures. For $x = 0.5$ the linewidth is nearly constant at about 2.3 kOe above T^*. Below T^* it decreases with decreasing temperature and increases again approaching $T_{N2} = 4.1$ K. Below the ordering temperature the resonance line can be followed much better than for the concentrations above. At $T = 2$ K it reaches $\Delta H = 3.4$ kOe. With increasing Ni concentration $x = 0.6$ and $x = 0.65$, the temperature dependence of the linewidth follows the pattern of $x = 0.5$, but the line broadening below T_{N2} becomes weaker and vanishes at $x = 0.7$. For x

$=0.8$ and $x = 1.0$, the linewidth strongly decreases with decreasing temperature below T^*, comparable to the behavior reported for the heavy-fermion compound CeCu$_2$Si$_2$.[8]

Depending on the temperature range, different information is obtained from the ESR linewidth ΔH. The decisive borderline is the magnetic-ordering temperature T_N of the compound under consideration. At temperatures $T < T_N$ the linewidth is dominated by inhomogeneous broadening due to internal magnetic fields which originate from the ordered Ce $4f$ moments. The incommensurate order of the Ce $4f$ moments gives rise to different internal fields at every Gd probe. This yields a broad distribution of resonance fields. The width of this distribution can be taken as a rough measure for the size of the ordered Ce $4f$ moment μ_{Ce}. Figure 4 reveals that for the sequence $x = 0.5$, 0.6, and 0.65 the size of the ordered moment decreases drastically due to Kondo compensation. Finally, for $x = 0.7$ no indications of a magnetic phase transition can be detected in $\Delta H(T)$.

At temperatures $T > T_N$ the linewidth reflects the transversal spin-relaxation rate $1/T_2 \propto \Delta H_R$ of the Gd spin. In metals the transversal relaxation time T_2 equals the longitudinal relaxation time T_1 which measures the spin-lattice relaxation. Therefore we obtain the spin-lattice relaxation directly from the linewidth data $\Delta H_R \propto 1/T_1$. Following Coldea et al., two decisive relaxation contributions determine the linewidth of intermetallic Ce compounds:[15]

$$\Delta H_R = \Delta H_K + \Delta H_{Ce}. \qquad (5)$$

The Korringa relaxation ΔH_K is caused by the exchange interaction between the Gd spin and the conduction electrons

and is usually observed in metals. It is linear in the temperature T:[11]

$$\Delta H_K = \frac{\pi k_B}{g\mu_B} \langle J^2_{Gd}(q)\rangle N^2(E_F)T = bT. \qquad (6)$$

$\langle J^2_{Gd}(q)\rangle$ is the exchange integral averaged over the momentum transfer q from the scattering of the conduction electrons at the Gd spin, and k_B denotes the Boltzmann constant. The second contribution ΔH_{Ce} takes the spin fluctuations of the Ce $4f$ moments (correlation time τ) into account, according to the fluctuation-dissipation theorem. These spin fluctuations are transferred to the Gd spin via RKKY interactions as an effective fluctuating magnetic field determined by the static Ce susceptibility χ^0_{Ce} and the RKKY coupling $\lambda^2_{CeGd}(R_i)$ summed up over the Ce moments at a distance R_i:[15]

$$\Delta H_{Ce} = \frac{2k_B}{g^2_{Ce}g_{Gd}\mu^3_B\hbar} T\chi^0_{Ce}\tau\sum_i \lambda^2_{CeGd}(R_i). \qquad (7)$$

For ideal heavy-fermion systems the Ce susceptibility χ^0_{Ce} follows a Curie-Weiss law $\chi^0_{Ce} \propto (T+\Theta)^{-1}$ with $\Theta = \sqrt{2}T^*$ (Ref. 16) at high temperatures $T > T^*$ and saturates as a large Pauli-like susceptibility ($\chi^0_{Ce} \to$ const) of heavy quasiparticles at $T \ll T^*$, where the Ce $4f$ moments are completely screened by the conduction electrons. Below T^* the Ce spin correlation time τ remains large and temperature independent at $\tau \approx h/k_BT^*$, whereas above T^* it decreases according to $1/\tau \propto \sqrt{T}$.[17] Assuming the Ce-Gd couplings $\lambda^2_{CeGd}(R_i)$ to be temperature independent, we simulated the temperature dependence of the linewidth for different characteristic temperatures T^* according to the compound $Ce(Cu_{1-x}Ni_x)_2Ge_2$. The typical Korringa contribution ΔH_K which is observed in these systems is of the order of $b \approx 5$ Oe/K.[8] The result of our calculation is shown in the lower frame of Fig. 5. At low temperatures $T \ll T^*$, the heavy Fermi liquid yields a strongly enhanced Korringa-like increase in ΔH. At temperatures near $T \approx T^*$, the spin fluctuations of the localized Ce moments become visible by the nonlinear curvature of $\Delta H(T)$. As both χ^0_{Ce} and τ decrease with increasing temperature, only the usual Korringa contribution ΔH_K remains at high temperatures $T \gg T^*$.

Our simulations qualitatively describe the temperature dependence of the linewidth data above the ordering temperature, as one can see in the upper frame of Fig. 5. The compounds $x=1.0$ and $x=0.8$ which show no magnetic ordering approximate the pattern for $T^*=30$ K and $T^*=15$ K, respectively. The behavior for $x=0.0$ is also reproduced using the appropriate $T^*=6$ K, but the decrease below T^* is suppressed in the experimental data by the inhomogeneous line broadening due to the magnetic ordering. With increasing T^* the compounds $x \geq 0.3$ allow one to distinguish the expected decrease of the spin-lattice relaxation below T^* from the inhomogeneous line broadening at the ordering temperature T_{N2}, as the linewidth exhibits a slight minimum between T^* and T_{N2}.

Because of the uncertainties concerning the determination of the crystal-field parameter b^0_2, which attains relatively large values, we avoided showing an exact fit of Eq. (5) to our data. However, to check the influence of a given crystal
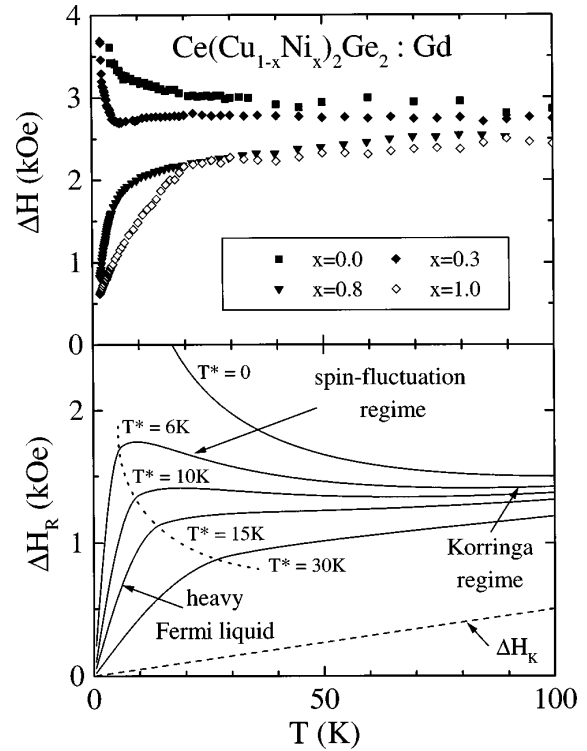

FIG. 5. Comparison of representative linewidth data at $\vartheta=90°$ (upper frame) with model calculations (lower frame) for different characteristic temperatures T^* following Eqs. (5)–(7). The parameters are given in the text.

field on the theoretical predictions, we simulated Eq. (4) for our experimental conditions ($\vartheta=90°$) using the typical heavy-fermion relaxation (5)–(7). We found that the crystal-field contribution—this is the third term in Eq. (4)—is nearly constant for temperatures $T > T^*$, where ΔH_R changes only slightly. Below T^* the decrease of ΔH_R with decreasing temperature increases the crystal-field term, but at the same time the second moment of all transitions decreases because of the temperature-dependent population of the Zeeman levels. This effect shifts the kink in $\Delta H(T)$, which is expected at T^* to lower temperatures, but maintains the characteristic pattern of heavy fermions.

IV. DISCUSSION

It seems interesting to compare our Gd^{3+} ESR results to results of NMR at the ^{63}Cu nuclear spin and to magnetic quasielastic neutron scattering (QNS) at the Ce spins. Figure 6 illustrates the different probes of the respective experiments and their couplings to the Ce spin. The NMR measures the nuclear spin-lattice relaxation rate $(1/T_1)_{NMR}$ of the ^{63}Cu nuclear spin **I** which—similar to the Gd^{3+} electron spin **S**—probes the fluctuations of the Ce spin **s** via RKKY-like interactions, where the electronic exchange integral J_{Gd} has to be replaced by the hyperfine coupling A of the nuclear copper spin to the electronic system. Therefore, comparable to ΔH_{ESR} in Eq. (5), the nuclear relaxation $(1/T_1)_{NMR}$ consists of the purely metallic Korringa relaxation $(1/T_1)_K$ and an additional contribution of the Ce $4f$ moments $(1/T_1)_{Ce}$.[18]

The double-differential cross section of the QNS at the Ce spins measures the dynamic structure factor $S(\mathbf{Q}, \omega, T)$ of the
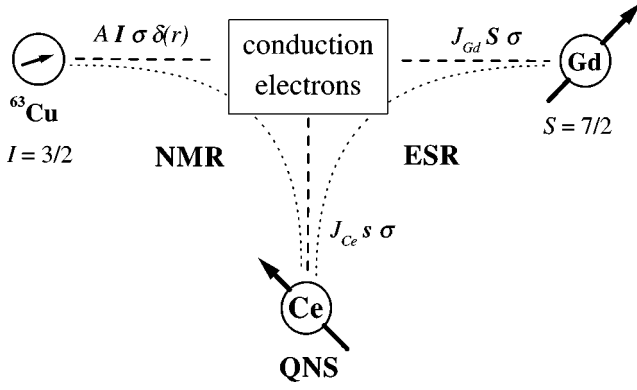
FIG. 6. Schematic representation of the probes for electron spin resonance (ESR), nuclear magnetic resonance (NMR), and quasielastic neutron scattering (QNS) and their respective couplings to the Ce $4f$ spin fluctuations.

electronic system. ω denotes the energy loss and $\mathbf{Q}$ the momentum transfer of the scattered neutrons. The fluctuation-dissipation theorem directly relates $S(\mathbf{Q},\omega,T)$ to the imaginary part of the dynamical Ce susceptibility $\chi_{Ce}(\mathbf{Q},\omega,T)$:[19]

$$S(\mathbf{Q},\omega,T) = \frac{\text{Im } \chi_{Ce}(\mathbf{Q},\omega,T)}{1 - \exp(-\hbar\omega/k_B T)}$$

$$\xrightarrow{k_B T \gg \hbar\omega} \frac{k_B T}{\hbar\omega} \text{ Im } \chi_{Ce}(\mathbf{Q},\omega,T). \qquad (8)$$

In principle, this is the basic relation which also describes the Ce contributions $(1/T_1)_{Ce}$ for ^{63}Cu NMR and ΔH_{Ce} for Gd^{3+} ESR, if we assume the hyperfine and RKKY couplings as temperature independent. The approximation $k_B T \gg \hbar\omega$ is fulfilled for low-neutron-energy transfers and for NMR and ESR experiments anyway. Using a purely relaxational ansatz and averaging over the momentum transfer $\mathbf{Q}$, the imaginary part of the dynamic susceptibility is a Lorentzian line centered at $\omega = 0$,

$$\text{Im } \chi_{Ce}(\omega,T) = \frac{\omega\Gamma}{\omega^2 + \Gamma^2} \chi_{Ce}^0, \qquad (9)$$

with the magnetic relaxation rate $\Gamma = 1/\tau$ (=quasielastic linewidth) and the static Ce susceptibility χ_{Ce}^0. For low-energy transfers compared to the quasielastic linewidth ($\omega \ll \Gamma$), we obtain the following expression which resembles Eq. (7):

$$S(\omega\to 0,T) \propto T \frac{\chi_{Ce}^0}{\Gamma} = T\tau\chi_{Ce}^0 \propto (1/T_1)_{Ce,NMR} \propto \Delta H_{Ce,ESR}. \qquad (10)$$

In Fig. 7 we plotted the neutron data[5] together with the ESR linewidth for the compounds $x=0$ and $x=1$. The temperature dependences of both observables coincide quite well. For $CeCu_2Ge_2$ the inhomogeneous line broadening of the ESR signal hides the decrease of the relaxation below the ordering temperature T_{N1}, which is observed by the neutron scattering. This decreasing relaxation below T_{N1} originates from a shift of the center of the quasielastic line $S(\mathbf{Q},\omega,T)$ from $\omega = 0$ to $\omega = \omega_M > 0$ due to the excitation energy of the magnetically ordered state. At high temperatures the ESR linewidth does not decrease as fast as the neutron data be-
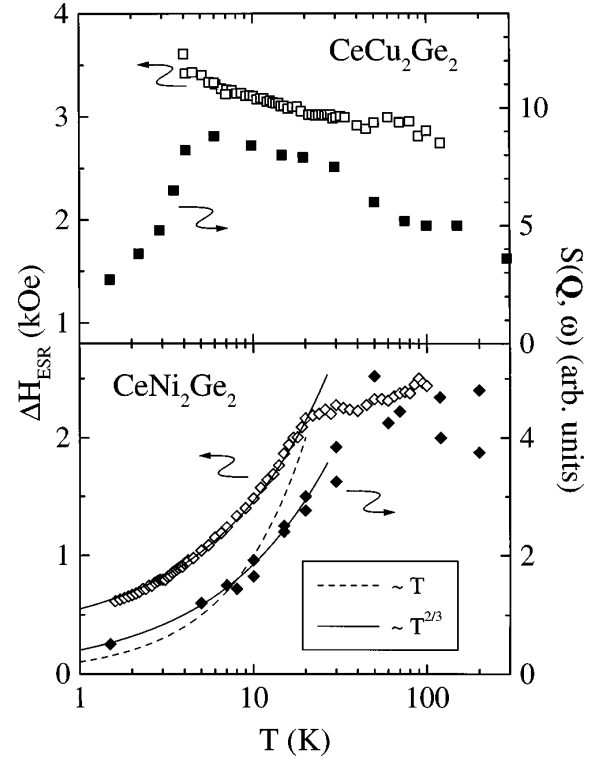

FIG. 7. Temperature dependence of the Gd^{3+} ESR linewidth ΔH_{ESR} (open symbols) for $x=0$ (upper frame) and $x=1$ (lower frame) compared to the QNS dynamic structure factor $S(\mathbf{Q},\hbar\omega=0.3 \text{ meV})$ (Ref. 5) (solid symbols). The dashed line indicates pure Korringa behavior. The solid lines correspond to a temperature dependence proportional to $T^{2/3}$ where a residual linewidth $\Delta H_0 = 0.4$ kOe was taken into account to fit the ESR data.

cause of the Korringa contribution ΔH_K, which increases linearly with the temperature. For $CeNi_2Ge_2$ the typical kink which marks the characteristic temperature T^* appears near 20 K in the ESR linewidth and around 30 K in the neutron data. This is not fully understood, but possibly it is in part due to the influence of the relatively strong crystal field on the ESR linewidth, which has been described at the end of the preceding section. However, it is interesting to note that ΔH as well as $S(\mathbf{Q},\omega)$ decreases weaker than linearly. A Korringa behavior $1/T_1 \propto T$ is indicated as a dashed line. These deviations from a linear increase may still result from quantum critical phenomena. Much more systematic work is needed to clarify this behavior in detail.

In Fig. 8 we compare the NMR relaxation rate of the compounds $x=0$ and $x=0.8$ (Refs. 20 and 5) to the respective ESR linewidth data. Again, the similarity of the temperature dependences is satisfying. For $CeCu_2Ge_2$ the decrease of the NMR relaxation rate below the ordering temperature is in accordance with the neutron scattering. At high temperatures the influence of the Korringa contribution becomes visible in the ESR linewidth rather than in the NMR relaxation rate for all the compounds. The relative strength of the Ce contribution compared to the normal Korringa relaxation is higher at the Cu site than at the Gd site, because the RKKY interaction which couples the respective probe to the Ce spin fluctuations strongly decreases with increasing distance R. As the nearest-neighbor distance between Cu and Ce is only about 3/4 of the Gd-Ce separation and the corre-
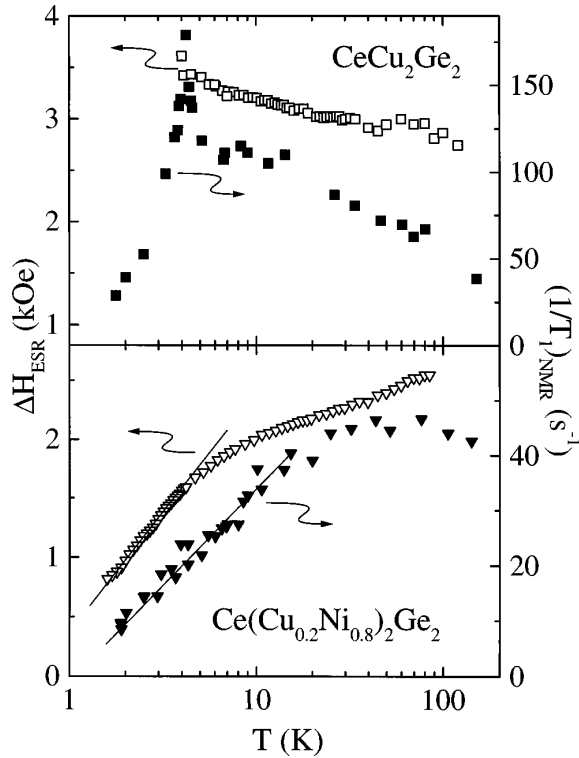
FIG. 8. Temperature dependence of the Gd^{3+} ESR linewidth ΔH_{ESR} (open symbols) for $x=0$ (upper frame) and $x=0.8$ (lower frame) compared to the ^{63}Cu NMR spin-lattice relaxation rate $(1/T_1)_{NMR}$ (Ref. 5) (solid symbols). The solid lines indicate a behavior proportional to $\ln(T/T_0)$.

FIG. 9. Temperature dependence of the Gd^{3+} ESR linewidth ΔH_{ESR} compared to the ^{63}Cu NMR linewidth ΔH_{NMR} (upper frame) and to the ^{63}Cu NMR spin-lattice relaxation rate $1/T_1$ (lower frame) for the concentration range $0.5 \le x \le 0.7$.

sponding squared matrix elements which determine the relaxation rate decrease proportional $1/R^6$,[21] one estimates a relative amplification of the Ce contribution by a factor of 5, if one changes from the Gd site to the Cu site.

The transition from magnetic order to Fermi-liquid behavior which develops with increasing x for the compounds $0.5 \le x \le 1.0$ is of special interest. Figure 9 compares both the NMR linewidth ΔH_{NMR} and spin-lattice relaxation rate $(1/T_1)_{NMR}$ to the ESR linewidth ΔH_{ESR}. For $x=0.5$, ΔH_{NMR} shows the same amount of inhomogeneous broadening below T_{N2} as ΔH_{ESR}. The NMR probe obviously detects the same distribution of internal fields due to the magnitude of the ordered moment μ_{Ce} as the ESR probe does. With increasing x the inhomogeneous broadening vanishes in both experiments, indicating the strong decrease of the ordered moment μ_{Ce} in accordance with the neutron diffraction.[1] Finally, for $x=0.7$ the ESR linewidth follows the NMR relaxation rate even below the ordering temperature T_{N2}. This observation supports the theory of a band magnetism of heavy quasiparticles[4] which was proposed to develop for concentrations $x>0.5$ and was characterized by small ordered moments and incommensurate propagation vectors.

Another interesting point is the non-Fermi-liquid behavior which is discussed for the compound $x=0.8$.[5] This compound is close to a quantum-phase transition, because the ordering temperature reaches zero, $T_{N2} \rightarrow 0$. The NMR spin-lattice relaxation rate shows a clear deviation from the linear Fermi-liquid dependence at low temperatures [Fig. 8 (Ref. 5)]. But there is still a lack of theory concerning this point in a non-Fermi liquid. The logar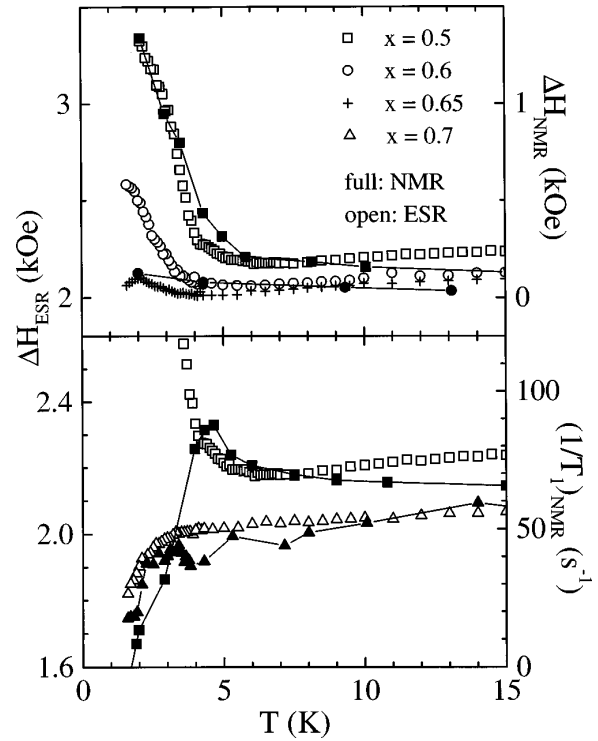ithmic temperature scale in Fig. 8 suggests $1/T_1 \propto \ln(T)$ for $T<15$ K. Further support was given by a logarithmic divergency in the Sommerfeld coefficient of the specific heat, $C/T \propto \ln(T)$, in the temperature range 1 K$\le T \le 6$ K,[6] which is in accordance to theoretical predictions. The ESR linewidth seems to support the NMR data (Fig. 8); however, the logarithmic temperature dependence develops only below $T<5$ K. Nevertheless, the logarithmic temperature axis (in Figs. 4, 7, and 8) stresses the different curvatures for $x=0.8$ and $x=1.0$ below T^*.

V. CONCLUSION

We have investigated the pseudoternary Kondo-lattice system $Ce(Cu_{1-x}Ni_x)_2Ge_2$ by Gd^{3+} ESR within the whole concentration range ($0 \le x \le 1$). The orientation dependence of the exchange narrowed ESR spectra has been explained by the influence of the dominantly uniaxial crystal field. With increasing x the development from magnetic order ($x=0$) to heavy-fermion behavior ($x=1$) is nicely probed by the Gd^{3+} ESR linewidth. Its temperature dependence above the ordering temperature T_N is well described by the Ce $4f$ spin fluctuations which are transferred to the Gd^{3+} spin via RKKY interactions. The onset of magnetic ordering (T_{N1}, T_{N2}) is characterized by a strong inhomogeneous line broadening due to internal fields connected with the incommensurate magnetic order of the Ce $4f$ moments. For $x>0.5$ the inhomogeneous broadening becomes weaker and reflects the decrease of the ordered Ce moment in accordance with the proposed transition from local moment to a band-type magnetism.

The comparison of the Gd^{3+} ESR linewidth with the ^{63}Cu NMR relaxation rate and the dynamic structure factor from quasielastic neutron scattering generally shows a qualitative agreement of the results above the ordering temperature ($T > T_N$) and establishes ESR as a useful tool to study the Ce spin dynamics. The quantitative differences have been attributed to the strong space dependence of the RKKY interaction and to the influence of the crystal field. For $T < T_N$ the ESR line broadening coincides very well with the NMR line broadening, which indicates that both probes detect the same internal field distribution due to the ordered Ce moment.

[1] A. Loidl, A. Krimmel, K. Knorr, G. Sparn, M. Lang, C. Geibel, S. Horn, A. Grauel, F. Steglich, B. Welslau, N. Grewe, H. Nakotte, F. R. de Boer, and A. Murani, Ann. Phys. (Leipzig) **1**, 78 (1992).

[2] N. Grewe and F. Steglich, *Handbook on the Physics and Chemistry of Rare Earths* (Elsevier Science, Amsterdam, 1991), Vol. 14.

[3] S. Doniach, Physica B **91**, 231 (1977).

[4] B. Welslau and N. Grewe, Physica B **165&166**, 387 (1990).

[5] N. Büttgen, R. Böhmer, A. Krimmel, and A. Loidl, Phys. Rev. B **53**, 5557 (1996).

[6] F. Steglich, P. Gegenwart, C. Geibel, R. Helfrich, P. Hellmann, M. Lang, A. Link, R. Modler, G. Sparn, N. Büttgen, and A. Loidl, Physica B **223&224**, 1 (1996).

[7] D. Jaccard, K. Behnia, and J. Sierro, Phys. Lett. A **163**, 475 (1992).

[8] M. Schlott, B. Elschner, M. Herrmann, and W. Assmus, Z. Phys. B **72**, 385 (1988).

[9] G. Feher and A. F. Kip, Phys. Rev. **98**, 337 (1955).

[10] F. J. Dyson, Phys. Rev. **98**, 349 (1955).

[11] S. E. Barnes, Adv. Phys. **30**, 801 (1981).

[12] S. E. Barnes, Phys. Rev. B **9**, 4789 (1974).

[13] T. Plefka, Phys. Status Solidi B **55**, 129 (1973).

[14] R. Spitzfaden, Ph.D. thesis, TU Darmstadt, 1996.

[15] M. Coldea, H. Schäffer, V. Weissenberger, and B. Elschner, Z. Phys. B **68**, 25 (1987).

[16] J. Callaway, *Quantum Theory of the Solid State* (Academic, New York, 1991), p. 448.

[17] D. L. Cox, N. E. Bickers, and J. W. Wilkins, J. Appl. Phys. **57**, 3166 (1985).

[18] M. J. Lysak and D. E. MacLaughlin, Phys. Rev. B **31**, 6963 (1985).

[19] M. Löwenhaupt and K. H. Fischer, *Handbook on the Physics and Chemistry of Rare Earths* (Elsevier Science, Amsterdam, 1993), Vol. 16.

[20] N. Büttgen, R. Böhmer, and A. Loidl, Solid State Commun. **93**, 753 (1995).

[21] D. L. Cox, Phys. Rev. B **35**, 6504 (1987).